SCIENCE CHINA
Information Sciences

• RESEARCH PAPER •

April 2016, Vol. 59 042303:1–042303:14
doi: 10.1007/s11432-015-5365-z

Self-mixed self-interference analog cancellation in full-duplex communications

Hongtao LU[1], Shihai SHAO[1*], Kai DENG[2] & Youxi TANG[1]

[1]*National Key Laboratory of Science and Technology on Communications, University of Electronic Science and Technology of China, Chengdu* 611731*, China;*
[2]*Department of Physical Science and Electronic Engineering, Yibin University, Yibin* 644000*, China*

Received June 15, 2015; accepted August 11, 2015; published online February 3, 2016

Abstract Rather than using existing self-interference cancellation methods, which essentially consist of reconstruction and subtraction, this paper proposes a novel approach, based on multiplication, to cancel self-interference in the analog domain in full-duplex communications. This approach is called self-mixed self-interference analog cancellation (SM-SIAC). Moreover, rather than using an individual analog cancellation circuit in existing self-interference cancellation methods, SM-SIAC can merge the analog cancellation circuit and the receiver. SM-SIAC is configured with three auto-tuning loops, consisting of one delay loop and two gain loops. SM-SIAC is further simplified with the Gaussian minimum shift keying (GMSK) self-interference signal. When these loops converge, the paper analyzes the cancellation capacity and derives a closed-form expression for the quadrature amplitude modulation self-interference signal and the GMSK self-interference signal. Simulation results illustrate the convergence of the gain loops and the cancellation capacity in the presence of engineering errors.

Keywords self-interference cancellation, full-duplex, self-mixed, analog cancellation, auto-tuning

Citation Lu H T, Shao S H, Deng K, et al. Self-mixed self-interference analog cancellation in full-duplex communications. Sci China Inf Sci, 2016, 59(4): 042303, doi: 10.1007/s11432-015-5365-z

1 Introduction

Currently, wireless radios using either the time-division approach or the frequency-division approach for bidirectional communications are generally in half-duplex mode. Hence, simultaneous reception and transmission in the same frequency band, i.e., full-duplex communication, can potentially double the throughput of half-duplex mode. Besides, full-duplex mode has advantages in overcoming thorny problems, such as hidden terminals, high end-to-end delays [1], and spectrum sensing in cognitive radio [2]. Due to these significant advantages, full-duplex communications have been attracting an increasing amount of research interest [3–20].

For full-duplex radio, the incoming composite signal consists of the user signal, the strong self-interference coupled from the transmit chain, and thermal noise. The most challenging problem is how to mitigate the destructive self-interference before the analog-to-digital converter (ADC) stage [4]. The cancellation is called analog cancellation. Ref. [3] reported an analog cancellation approach, shown in

* Corresponding author (email: ssh@uestc.edu.cn)

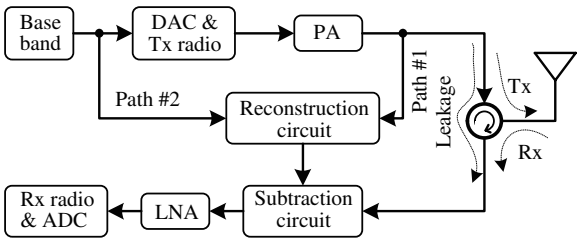

Figure 1 Existing approach for self-interference cancellation.

Figure 1, for narrowband systems. The approach follows path #1 and consists of two steps: (1) reconstructing a reference signal using the transmitted signal and (2) subtracting the reference signal from the incoming composite signal. Ref. [4] presented a different approach that follows path #2. Since then, the two approaches have dominated the development of full-duplex communications [1, 4–19].

Researchers [1, 13] have used the QHx220 [21] to reconstruct the reference signal. Researchers [10] have realized the subtraction operation using a Balun circuit, which inverts the reference signal instead of shifting its phase by π. This gave better cancellation capacity in the experiments. Refs. [4–9] couple the transmitted signal following path #2 and use an auxiliary transmit chain to up-convert the reference signal. In this mode, the reference signal is reconstructed in the digital domain, and various digital signal-processing algorithms [9] can be used to adjust the amplitude, the phase, and the delay. In contrast, Refs. [10–19] firmly follow path #1 and hardly take into account the noise and nonlinearities introduced by the transmit chain in the reference signal. In this case, the analog cancellation circuit contains one or several taps, each of which consists of a scaler device along with either a delay line or a phase shifter, or both. Ref. [11] realized self-interference reduction of 63 dB by employing up to 16 taps. All of these approaches are based on the reconstruction–subtraction operation, which does not make full use of the self-interference signal features to simplify the analog cancellation circuit and thus occupies additional printed circuit board area and consumes additional energy.

This paper proposes the self-mixed analog self-interference cancellation (SM-SIAC) method, which essentially is a combination of an analog cancellation circuit and a direct-conversion receiver [22, 23]. SM-SIAC uses two different methods for analog cancellation: (1) transforming the self-interference signal before the cancellation (no operation is applied on the self-interference signal before the subtraction operation in the existing analog cancellation approaches [11]) to obtain special characteristics and (2) merging the analog cancellation in the receiver (the analog cancellation circuit and receiver are individual systems in existing full-duplex radios [12]). SM-SIAC multiplies the transmitted signal by the received composite signal first and then employs three auto-tuning loops to maximize the cancellation performance. The *multiplication operation* is the biggest difference between SM-SIAC and the existing approaches. If the self-interference is a Gaussian minimum shift keying (GMSK) signal, SM-SIAC will be simplified considerably.

This paper is organized as follows. In Section 2, the proposed SM-SIAC approach is described in detail. Section 3 builds the auto-tuning loops. The performance analysis involving adjustment errors is carried out in Section 4. Section 5 gives the simulation results.

2 Self-mixed self-interference analog cancellation

For a full-duplex radio, the received composite signal contains the user signal and the self-interference signal leaking from its own transmitter, as shown in Figure 2. The two signals have the same statistical characteristics in both the frequency domain and the time domain, except for a large difference in power. The typical receiver sensitivity of a Wi-Fi radio is -90 dBm, which is up to 110 dB lower than its typical transmitting power of 20 dBm [24]. Considering that the circulator handles an isolation of 15 dB [11, 14], the residual self-interference is still 95 dB higher than the receiver sensitivity. Unfortunately, the ADC, typically found in commodity Wi-Fi radios [11], has a dynamic range of hardly 72 dB. This means that

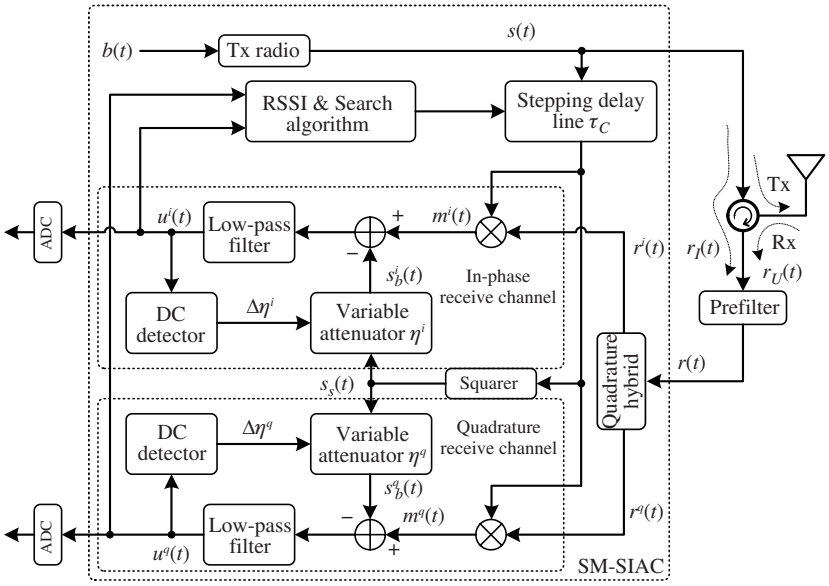

Figure 2 Block diagram of the proposed approach.

the user signal will be swamped completely by the quantization noise and thus the self-interference must be eliminated before the ADC stage [4, 25].

In Figure 2, the received composite signal is given by

$$r(t) = r_I(t) + r_U(t) + n(t), \tag{1}$$

where $r_I(t)$ represents the self-interference signal, $r_U(t)$ represents the user signal, and $n(t)$ represents thermal noise. The transmitted signal is given by

$$s(t) = \Re\{b(t)\exp(\mathrm{j}2\pi f_c t)\}, \tag{2}$$

where $b(t) = A(t)\exp[j\phi(t)]$ is a low-pass complex signal. The transmitted radio frequency signal in (2) couples into the receiver via the circulator. Thus, the self-interference signal is an attenuated and delayed version of the transmitted signal and is given by

$$r_I(t) = G_I s(t-\tau_I) = G_I \Re\{b(t-\tau_I)\exp[\mathrm{j}2\pi f_c(t-\tau_I)]\}. \tag{3}$$

The user signal at the receiver antenna is given by

$$r_U(t) = \Re\{b_U(t)\exp(\mathrm{j}2\pi f_c t)\}, \tag{4}$$

where $b_U(t) = A_U(t)\exp[\mathrm{j}\phi_U(t)]$ is its low-pass equivalent. Filtered by the prefilter, the thermal noise becomes a band-limited white Gaussian random process [26] and is given by

$$n(t) = \Re\{b_n(t)\exp(\mathrm{j}2\pi f_c t)\}, \tag{5}$$

where $b_n(t) = A_n(t)\exp[\mathrm{j}\phi_n(t)]$ is the low-pass equivalent of thermal noise. Substituting (3), (4), and (5) into (1) yields

$$r(t) = \Re\{[h_I b(t-\tau_I) + b_U(t) + b_n(t)]\exp(\mathrm{j}2\pi f_c t)\}, \tag{6}$$

where $h_I = G_I\exp(-\mathrm{j}2\pi f_c\tau_I)$ is the impulse response of the self-interference channel. In the SM-SIAC approach, the signal processing consists of four steps as follows.

1. A quadrature hybrid circuit splits the incoming signal into two parts with a 90-degree relative phase difference. Ignoring the power difference and the common phase shift, the two signals are given by

$$\begin{aligned} r^i(t) &= \Re\{[h_I b(t-\tau_I) + b_U(t) + b_n(t)]\exp(\mathrm{j}2\pi f_c t)\},\\ r^q(t) &= \Re\{[h_I b(t-\tau_I) + b_U(t) + b_n(t)]\exp(\mathrm{j}2\pi f_c t - \mathrm{j}\pi/2)\}, \end{aligned} \tag{7}$$

respectively.

2. The self-mixed signals, i.e., the product of the channel inputs and the τ_C-delayed replica of $s(t)$, are given by

$$m^i(t) = r^i(t)s(t-\tau_C), \quad m^q(t) = r^q(t)s(t-\tau_C). \tag{8}$$

Substituting (2) and (7) into (8) yields

$$\begin{aligned} m^i(t) = &\frac{1}{2}\Re\{[h_I b(t-\tau_I) + b_U(t) + b_n(t)]b^*(t-\tau_C)\exp(\mathrm{j}2\pi f_c\tau_C)\} + \\ &\frac{1}{2}\Re\{[h_I b(t-\tau_I) + b_U(t) + b_n(t)]b(t-\tau_C)\exp(\mathrm{j}4\pi f_c t - j2\pi f_c\tau_C)\}, \\ m^q(t) = &\frac{1}{2}\Re\left\{[h_I b(t-\tau_I) + b_U(t) + b_n(t)]b^*(t-\tau_C)\exp\left(\mathrm{j}2\pi f_c\tau_C - \mathrm{j}\frac{\pi}{2}\right)\right\} + \\ &\frac{1}{2}\Re\left\{[h_I b(t-\tau_I) + b_U(t) + b_n(t)]b(t-\tau_C)\exp\left(\mathrm{j}4\pi f_c t - \mathrm{j}2\pi f_c\tau_C - \mathrm{j}\frac{\pi}{2}\right)\right\}. \end{aligned} \tag{9}$$

3. The reference signals are the scaled versions of the squared $s(t-\tau_C)$ and are given by

$$\begin{aligned} s_b^i(t) &= \frac{1}{2}\eta^i s^2(t-\tau_C) = \frac{1}{2}\eta^i\|b(t-\tau_C)\|^2 + \frac{1}{2}\eta^i\Re\{b^2(t)\exp[\mathrm{j}4\pi f_c(t-\tau_C)]\}, \\ s_b^q(t) &= \frac{1}{2}\eta^q s^2(t-\tau_C) = \frac{1}{2}\eta^q\|b(t-\tau_C)\|^2 + \frac{1}{2}\eta^q\Re\{b^2(t)\exp[\mathrm{j}4\pi f_c(t-\tau_C)]\}, \end{aligned} \tag{10}$$

where η^i and η^q are the attenuator scalars.

4. The difference between the self-mixed signals and the reference signals is filtered by the low-pass filter, which is used to suppress the component centered at $2f_c$. The final outputs of SM-SIAC are given by

$$\begin{aligned} u^i(t) = &\ [m^i(t) - s_b^i(t)]\big|_{\text{low-pass filter}} \\ = &\frac{1}{2}\Re\{[h_I b(t-\tau_I) + b_U(t) + b_n(t)]b^*(t-\tau_C)\exp(\mathrm{j}2\pi f_c\tau_C) - \eta^i\|b(t-\tau_C)\|^2\}, \\ u^q(t) = &\ [m^q(t) - s_b^q(t)]\big|_{\text{low-pass filter}} \\ = &\frac{1}{2}\Re\{[h_I b(t-\tau_I) + b_U(t) + b_n(t)]b^*(t-\tau_C)\exp(\mathrm{j}2\pi f_c\tau_C - \mathrm{j}\pi/2) - \eta^q\|b(t-\tau_C)\|^2\}, \end{aligned} \tag{11}$$

which are fed to the ADC, subsequently. Combining the two signals in (11) yields a complex signal, which is given by

$$u(t) = u^i(t) + ju^q(t) = \beta(t) + \gamma(t) + \kappa(t), \tag{12}$$

where $\beta(t) = \frac{1}{2}\exp(\mathrm{j}2\pi f_c\tau_C)h_I b(t-\tau_I)b^*(t-\tau_C) - \frac{1}{2}\eta\|b(t-\tau_C)\|^2$ denotes the residual self-interference, $\gamma(t) = \frac{1}{2}\exp(\mathrm{j}2\pi f_c\tau_C)b_U(t)b^*(t-\tau_C)$ denotes the desired signal, $\kappa(t) = \frac{1}{2}\exp(\mathrm{j}2\pi f_c\tau_C)b_n(t)b^*(t-\tau_C)$ denotes the noise, and $\eta = \eta^i + \mathrm{j}\eta^q$.

3 Auto-tuning

There are three adjustment parameters to be tuned in SM-SIAC: (1) η^i for the in-phase receive channel, (2) η^q for the quadrature receive channel, and (3) τ_C for both. The objective is the power of the residual self-interference, i.e.,

$$\arg\min_{\tau_C,\eta^i,\eta^q} P_\beta, \tag{13}$$

where $P_\cdot$ represents the power of a signal. The solutions of (13) are

$$\begin{cases} \tau_C = \tau_I, \\ \eta = G_I. \end{cases} \tag{14}$$

Two gain loops and one delay loop are designed below to tune the adjustment parameters automatically.

3.1 Tuning the variable attenuators

For $\tau_C = \tau_I$, $u(t)$ is simplified and given by

$$u(t)|_{\tau_C=\tau_I} = \gamma(t) + \kappa(t) + \Delta\eta\|b(t-\tau_C)\|^2, \tag{15}$$

where $\Delta\eta = G_I - \eta$ is the unknown gain error $\Delta\eta$, and we will develop a special algorithm for it below.

The direct current (DC) component in $u(t)|_{\tau_C=\tau_I}$ is computed and given by

$$u_{\rm DC} = \lim_{a\to\infty}\frac{1}{2a}\int_{-a}^{a} u(t)|_{\tau_C=\tau_I}{\rm d}t = \Delta\eta\lim_{a\to\infty}\frac{1}{2a}\int_{-a}^{a}\|b(t-\tau_C)\|^2{\rm d}t = \Delta\eta R_b(0), \tag{16}$$

where $R_\cdot(\cdot)$ denotes the autocorrelation function of a signal and the subscript "DC" represents the DC component in a signal. $\Delta\eta$ is computed and given as

$$\Delta\eta = u_{\rm DC}/R_b(0) \;\Leftrightarrow\; \begin{cases} \Delta\eta^i = \Re\{u_{\rm DC}/R_b(0)\} = u^i_{\rm DC}/R_b(0), \\ \Delta\eta^q = \Im\{u_{\rm DC}/R_b(0)\} = u^q_{\rm DC}/R_b(0), \end{cases} \tag{17}$$

which is used to exploit two feedback loops, called gain loops. One gain loop tunes η^i, and the other tunes η^q. In each of the gain loops, the DC detector outputs the gain error, which the corresponding variable attenuator uses to change its own gain value. It is expected that, when the gain loops converge, the scalars of the two variable attenuators approach the optimal values, i.e., $\eta = G_I$.

3.2 Tuning the stepping delay line

For $\tau_C \neq \tau_I$, however, the gain loops converge to biased values, which are given in complex form by

$$\eta = \frac{\exp({\rm j}2\pi f_c\tau_C)h_I R_b(\tau)}{R_b(0)}, \tag{18}$$

where $\tau = \tau_C - \tau_I$ is the delay error. Eq. (18) shows that the gain loop errors depend on the delay error. When the gain loops converge, $u(t)$ becomes

$$u(t)|_{\eta\text{-cvg}} = \gamma(t) + \kappa(t) + h_I\exp({\rm j}2\pi f_c\tau_C)\left[b(t-\tau_I)b^*(t-\tau_C) - \frac{R_b(\tau)\|b(t-\tau_C)\|^2}{R_b(0)}\right], \tag{19}$$

the power of which is computed and given by

$$P_{u(t)|_{\eta\text{-cvg}}}(\tau) = P_\gamma + P_\kappa + G_I^2\lim_{a\to\infty}\frac{1}{2a}\int_{-a}^{a}\left\|b(t+\tau)b^*(t) - \frac{R_b(\tau)}{R_b(0)}\|b(t)\|^2\right\|^2{\rm d}t. \tag{20}$$

It is clear that $P_{u(t)|_{\eta\text{-cvg}}}(\tau)$ reaches the minimum $P_\gamma + P_\kappa$ when $\tau_C = \tau_I$. Therefore, the paper builds a feedback loop, called the delay loop, to tune the stepping delay line to approach the optimal delay τ_I.

3.3 Auto-tuning loops

There are bidirectional impacts between the gain loops and the delay loop. Hence, the auto-tuning process is a two-dimensional search problem. The block diagrams of the three loops are plotted in Figure 2. Note that the continuously variable attenuator is currently valid [27] and, consequently, the gain loops must be designed to make full use of the resolution. The processes in the gain loops are listed in Algorithm 1, which uses an integral circuit to realize the DC detection function. The two gain loops run in parallel in the analog domain entirely in the form of first-order feedback loops whose convergence condition is $G_D \in (0, 2/T_D/R_b(0))$. Unfortunately, it is hard to produce the precise variable delay line [11] at present. Cascading the stepping delay lines [28] and the fixed delay lines [29] gives a solution for the stepping delay line module, which handles a discrete time delay varying in a large range. A feasible search algorithm is to try all the valid delays of the stepping delay line. The detailed processes are listed in Algorithm 2.

Algorithm 1 Processes of the gain loops

Require: The DC detector gain $G_D > 0$, the integral time $T_D > 0$, the two variable attenuators $\eta^i = 0$ and $\eta^q = 0$, the thresholds V^i and V^q;

$n = 0$;
while 1 **do**
  $\Delta\eta^i \Leftarrow G_D \int_{nT_D}^{(n+1)T_D} u^i(t)\mathrm{d}t$, $\Delta\eta^q \Leftarrow G_D \int_{nT_D}^{(n+1)T_D} u^q(t)\mathrm{d}t$; % Realized by the DC detectors.
  if $\Delta\eta^i \leqslant V^i$ and $\Delta\eta^i \leqslant V^q$ **then**
    Break;
  end if
  $\eta^i \Leftarrow \eta^i + \Delta\eta^i$, $\eta^q \Leftarrow \eta^q + \Delta\eta^q$; % Realized by the variable attenuators.
  $u^i(t) = m^i(t) - \eta^i s_s(t)$, $u^q(t) = m^q(t) - \eta^q s_s(t)$; % Realized by the variable attenuators, subtractors, and low-pass filters.
  $n \Leftarrow n + 1$;
end while

Algorithm 2 Processes of the delay loop

Require: The power threshold $P_{\mathrm{th}} > 0$, the check period $T_p > 0$;

$\tau_{\mathrm{tmp}} \Leftarrow 0$;
$P_{u,\mathrm{tmp}} \Leftarrow 0$;
for each valid delay τ_C of the stepping delay line **do**
  $P_u \Leftarrow$ the output of the received signal strength indicator (RSSI) module;
  while 1 **do**
    $P_{u,\mathrm{last}} \Leftarrow P_u$;
    Delay T_p second; % Check for the convergence of the gain loops every T_p second.
    $P_u \Leftarrow$ the output of the RSSI module;
    if $\left|P_{u,\mathrm{last}} - P_u\right| \leqslant P_{\mathrm{th}}$ **then**
      Break;
    end if
  end while
  if $P_u < P_{u,\mathrm{tmp}}$ **then**
    $P_{u,\mathrm{tmp}} \Leftarrow P_u$;
    $\tau_{\mathrm{tmp}} \Leftarrow \tau_C$; % Record the optimal delay.
  end if
end for
Apply τ_{tmp} to the stepping delay line;

4 Performance analysis

The paper defines performance as the improvement of the signal to interference plus noise ratio (SINR) [4] when the auto-tuning loops converge. The SINRs for $r(t)$ and $u(t)$ are given by

$$\begin{cases} \mathrm{SINR}_r = \frac{P_{r_U}}{P_{r_I}+P_n}, \\ \mathrm{SINR}_u = \frac{P_\gamma}{P_\beta+P_\kappa}. \end{cases} \tag{21}$$

The cancellation capacity of SM-SIAC is computed and given by

$$G_c = \frac{\mathrm{SINR}_u}{\mathrm{SINR}_r} = \frac{P_\gamma(P_{r_I}+P_n)}{P_{r_U}(P_\beta+P_\kappa)} = \frac{2P_bP_{r_U}(P_{r_I}+P_n)}{P_{r_U}(P_\beta+2P_nP_b)} = \frac{1+\mathrm{NIR}}{\frac{P_\beta}{2P_{r_I}P_b}+\mathrm{NIR}}, \tag{22}$$

where $\mathrm{NIR} = P_n/P_{r_I}$ is the thermal noise to self-interference power ratio. From (3), we have $P_{r_I} = G_I^2P_b/2$. And substituting $P_b = R_b(0)$ and (18), we obtain that $P_\beta/2/P_{r_I}/P_b$ is the power of the normalized residual interference signal, which is given by

$$\Delta_r(t) = \frac{b(t+\tau)b^*(t) - R_b(\tau)\|b(t)\|^2/R_b(0)}{R_b(0)}. \tag{23}$$

Note that $\mathrm{NIR} \ll 1$ and, consequently, the performance is rewritten as

$$G_c = \left(P_{\Delta_r} + \mathrm{NIR}\right)^{-1}. \tag{24}$$

For $\tau = 0$, the cancellation capacity G_c reaches the upper bound

$$G_{c,\text{upper bound}} = \text{NIR}^{-1}. \tag{25}$$

The upper bound means that the residual self-interference reduces to the noise floor ideally. To obtain the general expression of the cancellation performance, the paper takes the quadrature amplitude modulation (QAM) signal and the GMSK signal as examples.

4.1 QAM signal

For a QAM signal, the low-pass equivalent signal of the transmitted signal is given by

$$b(t) = G_t \sum_n I_n p(t - nT), \tag{26}$$

where G_t is the amplitude gain of the transmitter, $\{I_n\}$ is an independent stationary information sequence with a normalized variance, T is the symbol interval, and $p(t)$ is the basic modulation pulse with an energy of T. Substituting (26) into (23) yields

$$\begin{aligned}\Delta_r(t) &= \sum_m \sum_n I_n I_m^* p(t+\tau-nT)p^*(t-mT) - \frac{R_b(\tau)}{R_b(0)} \sum_m \sum_n I_n I_m^* p(t-nT)p^*(t-mT) \\ &= \sum_\alpha \sum_n I_n I_{\alpha+n}^* p(t+\tau-nT)p^*(t-\alpha T-nT) - \frac{R_b(\tau)}{R_b(0)} \sum_\alpha \sum_n I_n I_{\alpha+n}^* p(t-nT)p^*(t-\alpha T-nT) \\ &= \sum_\alpha \sum_n w_{\alpha,n} p_{1,\alpha,\tau}(t-nT),\end{aligned} \tag{27}$$

where $w_{\alpha,n} = I_{\alpha+n}^* I_n$ is a new information element and $p_{1,\alpha,\tau}(t) = p^*(t-\alpha T)\left[p(t+\tau) - R_p(\tau)p(t)/T\right]$ is a new shaping pulse. It is clear that $\Delta_r(t)$ consists of component digital signals, each of which is defined as $\Delta_r^\alpha(t) = \sum_n w_{\alpha,n} p_{1,\alpha,\tau}(t-nT)$. Therefore, P_{Δ_r} is given by

$$P_{\Delta_r} = P_{\Delta_{r1}} + P_{\Delta_{r2}} + P_{\Delta_{r3}}, \tag{28}$$

where $P_{\Delta_{r1}} = \sum_{\alpha\neq 0} P_{\Delta_r^\alpha}$, $P_{\Delta_{r2}} = P_{\Delta_r^0}$, and $P_{\Delta_{r3}} = \sum_\alpha \sum_{\upsilon\neq\alpha} \lim\limits_{a\to\infty} \frac{1}{2a} \int_{-a}^{a} \Delta_r^\alpha(t)\Delta_r^{\upsilon *}(t)\mathrm{d}t$ is the cross item and shows the correlation between the component digital signals.

Considering $\Delta_r^\alpha(t)$ as a new linearly modulated signal and using the power spectral density (PSD) formulation of digital signals [26], $P_{\Delta_{r1}}$ is derived and given by

$$P_{\Delta_{r1}} = \sum_{\alpha\neq 0} \int_{-\infty}^{\infty} F_{\alpha,\tau}(f)\mathrm{d}f, \tag{29}$$

where $F_{\alpha,\tau}(f) = \left\|\mathcal{F}\left(p_{1,\alpha,\tau}(t)\right)\right\|^2/T$ and $\mathcal{F}(\cdot)$ represents the Fourier transform. Using the same method, $P_{\Delta_{r2}}$ is computed and given by

$$P_{\Delta_{r2}} = D(\|I_n\|^2) \int_{-\infty}^{\infty} F_{0,\tau}(f)\mathrm{d}f + \frac{1}{T}\sum_n F_{0,\tau}(nT), \tag{30}$$

where $D(\cdot)$ represents the variance of a random variable. $P_{\Delta_{r3}}$ is derived and given by

$$P_{\Delta_{r3}} = 2\sum_{\alpha=1}^{\infty} \Re\left\{R_{p_{2,\tau}}(\alpha T)\right\}, \tag{31}$$

where $R_{p_{2,\tau}}(\cdot)$ is the autocorrelation function of $p_{2,\tau}(t) = p(t)\left[p(t+\tau) - R_p(\tau)p(t)/T\right]$. Substituting (29) into (31), the cancellation capacity G_c in (22) is written as

$$\begin{aligned}G_c = \Bigg\{ &\sum_{\alpha\neq 0} \int_{-\infty}^{\infty} F_{\alpha,\tau}(f)\mathrm{d}f + D(\|I_n\|^2) \int_{-\infty}^{\infty} F_{0,\tau}(f)\mathrm{d}f \\ &+ \frac{1}{T}\sum_n F_{0,\tau}(nT) + 2\sum_{\alpha=1}^{\infty} \Re\left\{R_{p_{2,\tau}}(\alpha T)\right\} + \text{NIR} \Bigg\}^{-1}.\end{aligned} \tag{32}$$

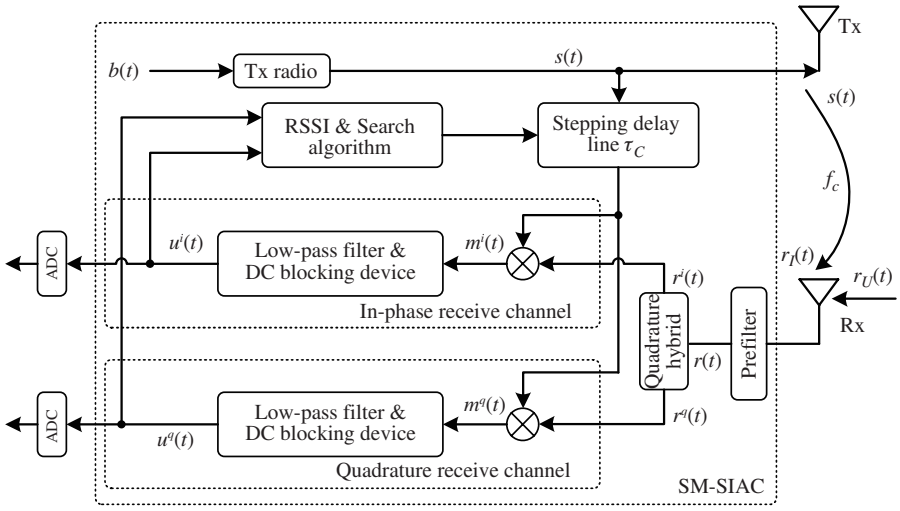

Figure 3 Simplified block diagram of the proposed approach for a GMSK signal.

4.2 GMSK signal

The GMSK signal [30] is given by

$$b(t) = G_t \exp\left(\mathrm{j}2\pi h \int_{-\infty}^{t} \sum_n I_n g(t_1 - nT)\mathrm{d}t_1\right), \quad I_n \in \{-1,\ 1\}, \tag{33}$$

where $h = 0.5$ is the modulation index. Since the GMSK signal has a constant envelope, the block diagram of SM-SIAC is simplified and plotted in Figure 3. The squarer device and the gain loops are removed. Only two DC blocking devices are used to filter out the self-interference energy. Eq. (23) becomes

$$\Delta_r(t) = \left.\frac{b(t+\tau)b^*(t)}{R_b(0)}\right|_{\text{DC block}}, \tag{34}$$

when DC blocking devices are used instead of the gain loops. Substituting (33) into (34) yields

$$\begin{aligned}
\Delta_r(t) &= \exp\left[\mathrm{j}2\pi h\left(\int_{-\infty}^{t+\tau}\sum_n I_n g(t_1 - nT)\mathrm{d}t_1 - \int_{-\infty}^{t}\sum_n I_n g(t_1 - nT)\mathrm{d}t_1\right)\right]\Bigg|_{\text{DC block}} \\
&= \exp\left[\mathrm{j}2\pi h\left(\int_{-\infty}^{t}\sum_n I_n g(t_1 + \tau - nT)\mathrm{d}t_1 - \int_{-\infty}^{t}\sum_n I_n g(t_1 - nT)\mathrm{d}t_1\right)\right]\Bigg|_{\text{DC block}} \\
&= \exp(\mathrm{j}\phi_\tau(t))|_{\text{DC block}},
\end{aligned} \tag{35}$$

where

$$\begin{aligned}
\phi_\tau(t) &= 2\pi h \int_{-\infty}^{t}\sum_n I_n(g(t_1 + \tau - nT) - g(t_1 - nT))\mathrm{d}t_1 \\
&= 2\pi h \sum_n I_n\left(\int_{-\infty}^{t+\tau-nT} g(t_1)\mathrm{d}t_1 - \int_{-\infty}^{t-nT} g(t_1)\mathrm{d}t_1\right) \\
&\approx 2\pi h\tau \sum_n I_n g(t - nT).
\end{aligned} \tag{36}$$

Ref. [28] gives a delay line with a step interval of 0.1 ns, which is far smaller than the symbol interval in the existing communication systems, such as GSM. In that case, $\phi_\tau(t)$ is very small and

$$\Delta_r(t) = [\cos(\phi_\tau(t)) + j\sin(\phi_\tau(t))]|_{\text{DC block}} \approx j\phi_\tau(t). \tag{37}$$

Combining (36) and (37), we have

$$P_{\Delta_r} = \frac{4\pi^2 h^2 \int_{-\infty}^{\infty} g^2(t)\mathrm{d}t}{T}\tau^2. \tag{38}$$

Then, the performance becomes

$$G_c = \left\{ \frac{4\pi^2 h^2 \int_{-\infty}^{\infty} g^2(t)\mathrm{d}t}{T}\tau^2 + \mathrm{NIR} \right\}^{-1}, \tag{39}$$

where $\int_{-\infty}^{\infty} g^2(t)\mathrm{d}t$ can be computed using numerical computation methods.

5 Simulation results

In this section, we present some simulation results to verify the analysis in Section 4 with engineering errors. The carrier frequency is 2 GHz. The powers for $r_U(t)$, $r_I(t)$, and $n(t)$ are set to -70 dBm, 0 dBm, and -80 dBm, respectively. In that case, we have NIR $= -80$ dB.

5.1 Simulations for the QAM signal

For a QAM signal, two problems need to be considered: (1) the finite integral time and detector gain of the DC detectors and (2) the timing error resulting from the step interval. The simulations use the 64-QAM constellation and a square root raised cosine pulse with a roll-off factor of 0.22. The gain loops employ two voltage variable attenuators, which are valid currently.

5.1.1 *Finite integral time and detector gain of the DC detector*

In practice, the two DC detectors integrate $u^i(t)$ and $u^q(t)$, respectively, in which there exists a strong alternating current component. Consequently, for finite integral time T_D, $\Delta\eta^i$ and $\Delta\eta^q$ contain residual alternating current components, which act as random errors. Moreover, each of the gain loops is essentially a first-order loop and, consequently, the detector gain G_D must be considered. Therefore, we give some simulation results in Figure 4 where the self-interference bandwidth is 20 MHz and the step interval of the stepping delay line is 0.1 ns.

To illustrate intuitively the impact of the finite integral time, we run the simulation 100 times for each integral time T_D and plot all the 100 results in Figure 4 (a) and (c). For a shorter integral time, the simulated results scatter in a larger range because the DC detector output error is stronger and vice versa. For a fixed integral time, the scattering range enlarges as the timing error increases. Moreover, a bigger detector gain results in a larger scattering range. In Figure 4 (b) and (d), the gain loops converge as the time increases. It is clear that the gain loops cost less time before converging when either the detector gain increases or the timing error decreases. These simulated results illustrate that the detector gain G_D and the integral time T_D must be designed carefully to realize the tradeoff between performance and the convergence speed of the gain loops.

5.1.2 *Step interval of the stepping delay line*

For the delay loop, the problem is whether Algorithm 2 yields the optimal delay or not. Note that the step interval of the stepping delay line results in an inevitable timing error, which decreases the performance. In Figure 5, the simulations employ a delay line with a step interval of 0.4 ns, an integral time of 1ns in the DC detectors, and self-interference with a bandwidth of 20 MHz. They are executed for 100 times for each timing error τ. For the unknown self-interference channel, the best alignment is that the self-interference delay τ_I is located exactly at a valid delay of the stepping delay line. For that case, the simulated results are shown in Figure 5 (a) and (c). Algorithm 2 can separate the optimal value easily. The worst alignment is that the self-interference delay τ_I is located at the middle of a step interval. In Figure 5(b), the optimal value and the suboptimal value are still separable. However, the

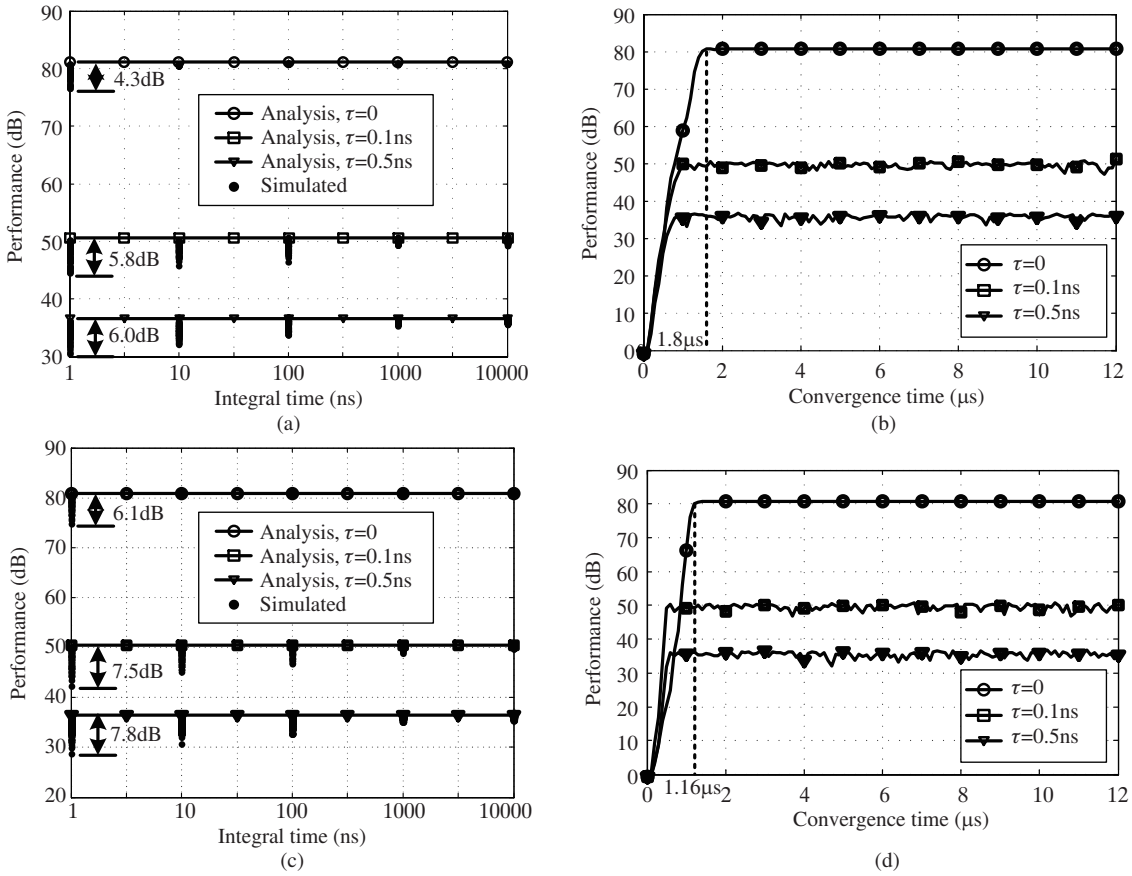

Figure 4 (a) Performance G_c vs. integral time T_D for different timing errors τ for detector gain $G_D = 0.5$; (b) performance G_c when the gain loops converge for different timing errors τ for integral time $T_D = 100$ ns and detector gain $G_D = 0.5$; (c) performance G_c vs. integral time T_D for different timing errors τ for detector gain $G_D = 0.6$; (d) performance G_c when the gain loops converge for different timing errors τ for integral time $T_D = 100$ ns and detector gain $G_D = 0.6$.

scattering range for the optimal value and that for the suboptimal value overlap in Figure 5(d). That means that Algorithm 2 probably outputs a suboptimal value but not the optimal value. To avoid this mistake, the scattering range must be narrowed to a tolerable range. The tolerable ranges for different step intervals are plotted in Figure 6. It is clear that a step interval of 0.4 ns results in a tolerable range of 9.5 dB, which is smaller than the scattering range 10.9 dB in Figure 5(d). That is why the error occurs. If the step interval is greater than 0.04 ns, the tolerable range is no less than 9.4 dB. However, when the step interval is smaller than 0.04 ns, the tolerable range quickly approaches 0, which means a quickly increased requirement for the gain loop design. Figure 6 gives a reference for the designer to determine the requirement for the gain loops. Although the above results are computed using self-interference with a bandwidth of 20 MHz, the curve in Figure 6 is independent of the self-interference bandwidth.

Figure 7 gives some simulated results to illustrate the effect of the self-interference bandwidth on the performance for different timing errors. When the timing error equals 0, the self-interference bandwidth has no effect on the performance. However, the timing error is always non-zero in practice and the performance will degrade as the self-interference bandwidth increases. For self-interference with a bandwidth of 20 MHz, a timing error of 0.1 ns results in a performance degradation of about 30 dB, from 80 dB down to 50 dB. This shows that the performance of broadband self-interference is more sensitive to the timing error than that of the narrowband self-interference.

5.2 Simulations for the GMSK signal

If a full-duplex radio transmits a GMSK signal, the SM-SIAC block diagram is greatly simplified. The most obvious feature is that the gain loops are removed. Hence, the stepping delay line is the sole

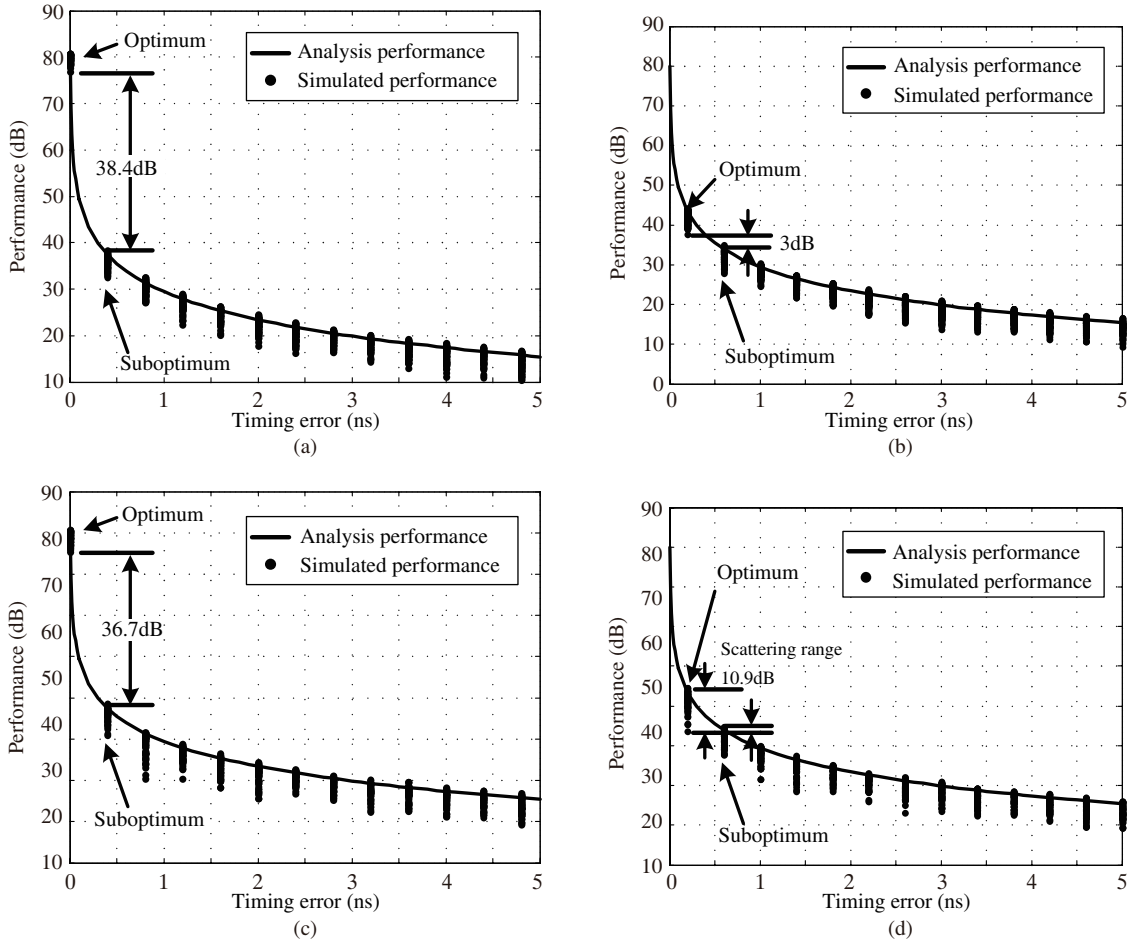

Figure 5 (a) Performance with various timing delays with $G_D = 0.5$ and the best alignment; (b) performance with various timing delays with $G_D = 0.5$ and the worst alignment; (c) performance with various timing delays with $G_D = 0.6$ and the best alignment; (d) performance with various timing delays with $G_D = 0.6$ and the worst alignment.

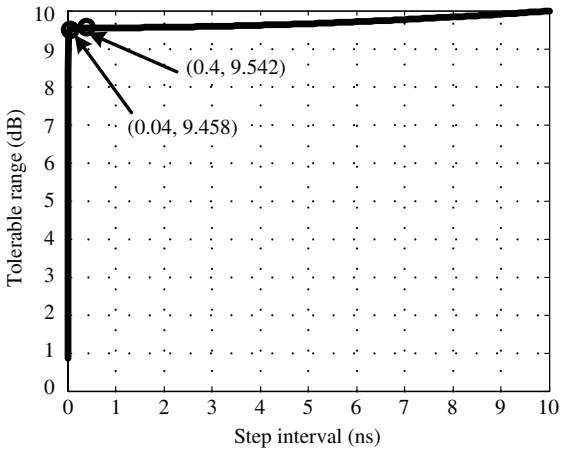

Figure 6 Tolerable range vs. step interval of the stepping delay line.

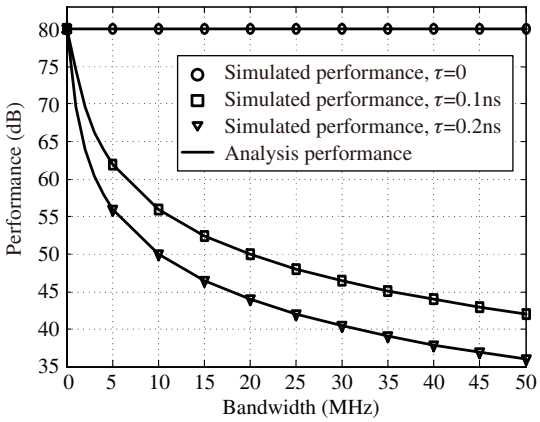

Figure 7 Performance vs. self-interference bandwidth for different timing errors τ.

adjusting device. In the simulations below, the symbol interval T is set to 50 ns.

For a step interval of 0.4 ns, the simulated results for the best alignment and the worst alignment are plotted in Figure 8, with the normalized premodulation filter bandwidth BT = 0.3. Because the gain loops are replaced by the DC blocking devices, Algorithm 2 will always yield the optimal delay if the RSSI outputs a sufficiently accurate power value. In Figure 8 (a) and (b), the errors in the RSSI outputs

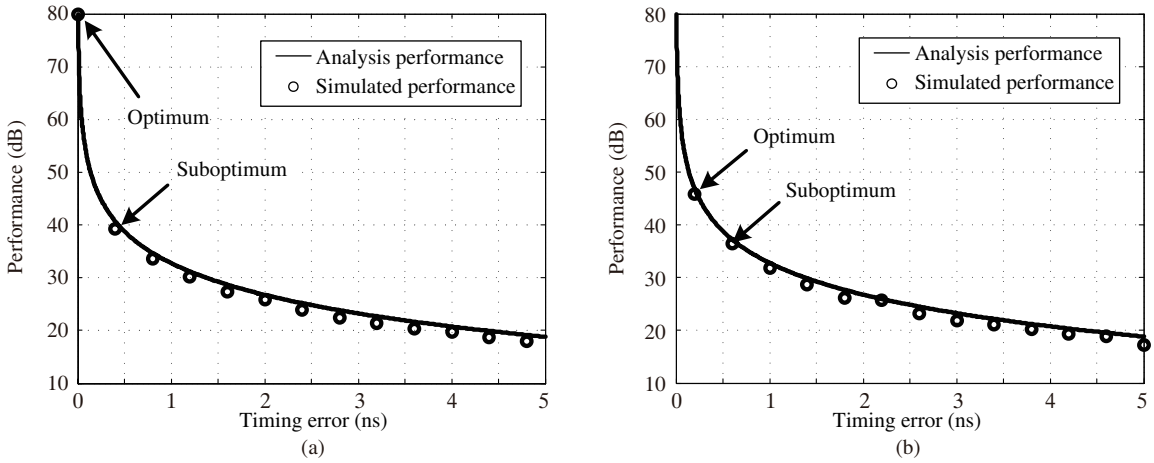

Figure 8 (a) Best case with a GMSK signal; (b) worst case with a GMSK signal.

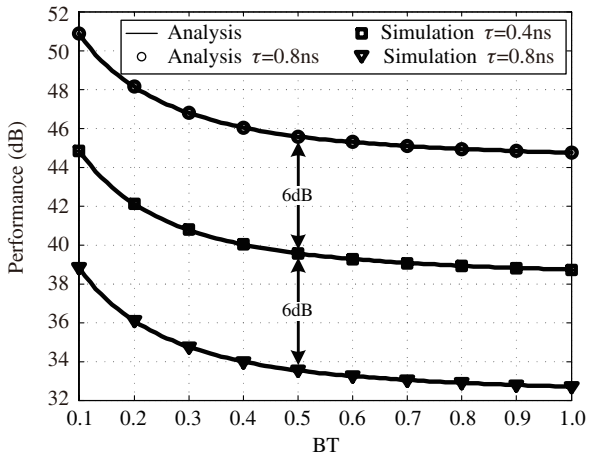

Figure 9 Performance vs. BT with a GMSK signal.

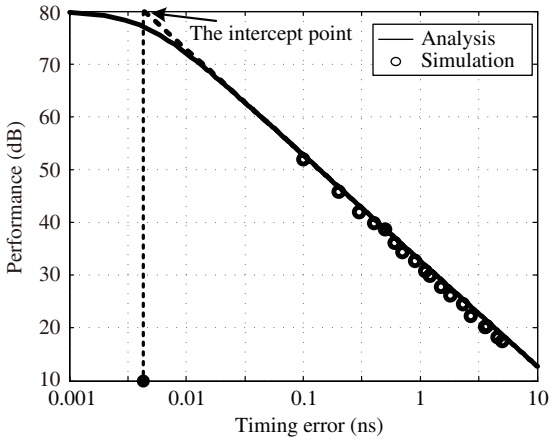

Figure 10 Performance vs. timing error with a GMSK signal.

are not big enough to make the optimal delay and the suboptimal delay inseparable.

The GMSK frequency shaping pulse $g(t)$ for various normalized premodulation filter bandwidths BT are plotted in [31]. A smaller BT means a "fatter" $g(t)$, which has less energy than the "thinner" ones. This is the reason why the performance increases as BT decreases in Figure 9. Figure 10 illustrates the linear relationship between the timing error τ and the performance G_c in (39).

5.3 Comparison with existing methods

A comparison between the SM-SIAC method and the existing methods, the ones reported in [1, 4, 11], is shown in Table 1. The advantages of SM-SIAC are as follows:

1. SM-SIAC realizes the analog cancellation and down-conversion simultaneously, which reduces the hardware complexity considerably.

2. Since it uses the characteristics of self-interference, SM-SIAC and the method in [3] are suitable for specialized radios.

3. The gain loops run in the analog domain and thus they are easily integrated.

4. SM-SIAC does not require the reference signal to have the same power as self-interference and this therefore reduces the transmitted power.

Consequently, SM-SIAC is attractive for small and low-power full-duplex devices, especially for GMSK radios.

Table 1 Comparison with existing methods

Items	SM-SIAC	Single-tap [1]	Auxiliary Tx chain [4]	Multi-taps [11]
1. Functions	Analog cancellation and down-conversion	Analog cancellation	Analog cancellation	Analog cancellation
2. Need additional down-conversion circuits in the receiver?	No	Yes	Yes	Yes
3. Uses the characteristics of self-interference?	Yes	No	Yes	No
4. In which domain does the auto-tuning algorithm run?	Analog and digital domains	Digital domain	Digital domain	Digital domain
5. Hardware complexity of the receiver	Low	Medium	Medium	High
6. Tx power reduction	Low	Medium	Zero	High
7. Thermal noise increment	Low	Low	Low	High
8. Power consumption	Low	Medium	Medium	High
9. Application scenarios	Single-path	Single-path	Multi-path	Multi-path
10. Most suitable modulation mode	GMSK	All existing modulation modes	Orthogonal frequency division multiplexing	All existing modulation modes
11. Analog cancellation performance	Low	Low	Low	High

6 Conclusion

This paper proposes two novel methods for self-interference cancellation in full-duplex communications. Following the two methods, a realistic cancellation technique, SM-SIAC, is described and analyzed. The auto-tuning loops are analyzed with engineering errors. Taking the QAM signal and the GMSK signal as examples, the paper derives the closed-form performance expression for SM-SIAC where the SINR improvement is used as the metric. The simulation results illustrate the operations and the effects of the auto-tuning loops and the delay loop. In the SM-SIAC approach, the functions of the direct-conversion receiver and self-interference analog cancellation are merged, which reduces costs and circuit complexity. The self-mixed operation allows the gain loops to operate completely in the analog domain and, consequently, reduces the auto-tuning complexity significantly.

Acknowledgements This work was supported by National Natural Science Foundation of China (Grant Nos. 61271164, 61471108, 61201266), National Major Projects (Grant No. 2014ZX03003001-002), and National High-tech R&D Program of China (863 Program) (Grant Nos. 2014AA01A704, 2014AA01A706).

Conflict of interest The authors declare that they have no conflict of interest.

References

1 Choi J I, Jain M, Srinivasan K, et al. Achieving single channel, full duplex wireless communication. In: Proceedings of 16th Annual International Conference on Mobile Computing and Networking (MOBICOM'10), New York, 2010. 1–12
2 Yin W S, Ren P Y, Li F, et al. Joint sensing and transmission for AF relay assisted PU transmission in cognitive radio networks. IEEE J Sel Areas Commun, 2013, 31: 2249–2261
3 Chen S, Beach M A, McGeehan J P. Division-free duplex for wireless applications. Electron Lett, 2002, 34: 147–148
4 Sahai A, Patel G, Sabharwal A. Pushing the Limits of Full-Duplex: design and Real-Time Implementation. Rice University Technical Report Networking and Internet Architecture (cs.NI). 2011
5 Duarte M, Sabharwal A. Full-duplex wireless communications using off-the-shelf radios: feasibility and first results. In: Proceedings of 44th Asilomar Conference on Signals, Systems and Computers (ASILOMAR), Pacific Grove, 2010. 1558–1562

6 Duarte M, Dick C, Sabharwal A. Experiment-driven characterization of full-duplex wireless systems. IEEE Trans Wirel Commun, 2012, 11: 4296–4307
7 Ahmed E, Eltawil A M, Sabharwal A. Rate gain region and design tradeoffs for full-duplex wireless communications. IEEE Trans Wirel Commun, 2013, 12: 3556–3565
8 Zhan Z, Villemaud G, Gorce J M. Design and evaluation of a wideband full-duplex OFDM system based on AASIC. In: Proceedings of IEEE 24th International Symposium on Personal Indoor and Mobile Radio Communications (PIMRC), London, 2013. 68–72
9 Duarte M, Sabharwal A, Aggarwal V, et al. Design and characterization of a full-duplex multiantenna system for WiFi networks. IEEE Trans Veh Technol, 2014, 63: 1160–1177
10 Jain M, Choi J I, Kim T, et al. Practical, real-time, full duplex wireless. In: Proceedings of 17th Annual International Conference on Mobile Computing and Networking (MOBICOM'11), New York, 2011. 301–312
11 Bharadia D, Mcmilin E, Katti S. Full duplex radios. In: Proceedings of ACM SIGCOMM 2013 Conference (SIGCOMM'13), New York, 2013. 375–386
12 Bharadia D, Katti S. Full duplex MIMO radios. In: Proceedings of 11th USENIX Symposium on Networked Systems Design and Implementation (NSDI'14), Seattle, 2014. 359–372
13 Radunovic B, Gunawardena D, Key P, et al. Rethinking indoor wireless mesh design: low power, low frequency, full-duplex. In: Proceedings of IEEE Workshop on Wireless Mesh Networks (WIMESH 2010), Boston, 2010. 1–6
14 Hong S S, Mehlman J, Katti S. Picasso: flexible RF and spectrum slicing. In: Proceedings of ACM SIGCOMM Computer Communication Review—Special October Issue (SIGCOMM'12), New York, 2012. 37–48
15 Hong S, Mehlman J, Katti S. Picasso: full duplex signal shaping to exploit fragmented spectrum. In: Proceedings of 10th ACM Workshop on Hot Topics in Networks, New York, 2011. 16
16 McMichael J G, Kolodziej K E. Optimal tuning of analog self-interference cancellers for full-duplex wireless communication. In: Proceedings of 50th Annual Allerton Conference on Communication, Control, and Computing (Allerton), Monticello, 2012. 246–251
17 Choi Y S, Mehr H S. Simultaneous transmission and reception: algorithm, design and system level performance. IEEE Trans Wirel Commun, 2013, 12: 5992–6010
18 Meerasri P, Uthansakul P, Uthansakul M. Self-interference cancellation-based mutual-coupling model for full-duplex single-channel MIMO systems. Int J Antennas Propag, 2014, 2014: 405487
19 Hua Y B, Liang P, Ma Y M, et al. A method for broadband full-duplex MIMO radio. IEEE Signal Process Lett, 2012, 19: 793–796
20 Cheng W C, Zhang H L. Quality-of-service driven power allocations for wireless full-duplex bidirectional links. Sci China Inf Sci, 2014, 57: 042316
21 Intersil LLC. Active isolation enhancer and interference canceller QHx220. 2009. http://www.intersil.com/en/products/other-analog/noise-canceller/isolation-enhancer-noise-cancellation/QHX220.html
22 Abidi A A. Direct-conversion radio transceivers for digital communications. IEEE J Solid-State Circ, 1995, 30: 1399–1410
23 Razavi B. Design considerations for direct-conversion receivers. IEEE Trans Circ Syst II, 1997, 44: 428–435
24 Bardwell J. WiFi radio characteristics and the cost of WLAN implementation: a tutorial, comparing and contrasting the use of consumer-grade and commercial-grade equipment. Connect802 Corporation Technical Report. 2005
25 Li N, Zhu W H, Han H H. Digital interference cancellation in single channel, full duplex wireless communication. In: Proceedings of 8th International Conference on Wireless Communications, Networking and Mobile Computing (WiCOM), Shanghai, 2012. 1–4
26 Couch L W. Digital and Analog Communication Systems. New Jersey: Prentice-Hall, 1996. 495–496
27 Analog Devices. HMC346LC3B GaAs MMIC voltage-variable attenuator. http://www.analog.com/media/en/technical-documentation/data-sheets/hmc346lc3b.pdf
28 Susumu Inc. GL1L SOP thin film differential delay line. http://www.susumu-usa.com/pdf/products_40.pdf
29 Anaren Inc. Model XDL09-9-204 delay line. http://www.anaren.com/products/delay-lines
30 Murota K, Hirade K. GMSK modulation for digital mobile radio telephony. IEEE Trans Commun, 1981, 29: 1044–1050
31 Stüber G L. Principles of Mobile Communication. New York: Springer, 2012. 228–231